

A mathematical perspective on edge-centric functional connectivity

Leonardo Novelli^{1,*} and Adeel Razi^{1,2,3}

¹*Turner Institute for Brain and Mental Health, School of Psychological Sciences and Monash Biomedical Imaging, Monash University, Australia*

²*Wellcome Centre for Human Neuroimaging, University College London, United Kingdom*

³*CIFAR Azrieli Global Scholars Program, CIFAR, Toronto, Canada*

(Dated: June 22, 2021)

Edge-centric functional connectivity (eFC) has recently been proposed to characterise the finest time resolution on the FC dynamics without the concomitant assumptions of sliding-window approaches. Here, we lay the mathematical foundations for the edge-centric analysis and examine its main findings from a quantitative perspective. The proposed framework provides a theoretical explanation for the observed occurrence of high-amplitude edge cofluctuations across datasets and clarifies why a few large events drive the node-centric FC (nFC). Our exposition also constitutes a critique of the edge-centric approach as currently applied to functional MRI (fMRI) time series. The central argument is that the existing findings based on edge time series can be derived from the static nFC under a null hypothesis that only accounts for the observed static spatial correlations and not the temporal ones. Challenging our analytic predictions against fMRI data from the Human Connectome Project confirms that the nFC is sufficient to replicate the eFC matrix, the edge communities, the large cofluctuations, and the corresponding brain activity mode. We conclude that the temporal structure of the edge time series has not so far been exploited sufficiently and encourage further work to explore features that cannot be explained by the presented static null model.

I. INTRODUCTION

Edge-centric functional connectivity (eFC) analysis [1, 2] has generated renewed excitement in the network neuroscience community as it provides the finest time resolution on the node-centric FC (nFC) dynamics without the additional assumptions required by sliding-window approaches [3, 4]. While the potential of eFC continues to be explored [5, 6], there is a consensus on the need for appropriate statistical tests and null models [2, 5]. The first concern is that the high-amplitude cofluctuations in the cortical activity that drive the nFC could be artefacts, potentially specific to fMRI. This has been mitigated by evidence showing that the high-amplitude events in the root-sum-of-squares (RSS) of the edge time series are not systematically related to confounding variables including in-scanner motion, respiratory and heart rate [1]. Furthermore, similar large events can be observed in synthetic time series, suggesting they are not intrinsic to fMRI nor other neuroimaging modalities [7]. These studies present evidence for the role of the edge-centric approach as a promising bridge between structure and function.

On the other hand, several widely-acknowledged publications have warned about the dangers of extracting structure from noise when studying static or dynamic FC, often using minimal null models to reproduce existing results [8–13]. The warnings concerning sampling variability also concern the edge-centric methods, particularly since high-amplitude RSS fluctuations can be observed in temporally-uncorrelated synthetic time series. Indeed, accounting for static spatial correlations is sufficient to

replicate key empirical findings [1, Fig. S4]. This observation has been interpreted as further evidence that large RSS fluctuations are not fMRI artefacts. However, it arguably raises an equally pressing conceptual concern: does the edge-centric approach provide statistical information about the time-varying connectivity that cannot be explained by the nFC?

Here, we tackle this question mathematically and provide a theoretical explanation for the widespread occurrence of large cofluctuations across datasets, and why a few large events drive the nFC. These rest on fundamental properties of subexponential distributions and large deviations theory [14, 15]. Additional derivations clarify how the nFC eigenvalues shape the RSS distribution and how the leading nFC eigenvectors underpin the spatial modes expressed during high-amplitude events. The influence of functional modules on the eigenvalue distribution could thus explain why the RSS events disappear when the modular structure is disrupted, as recently reported in [7]. Finally, we analytically show that the eFC matrix, the edge communities, the large cofluctuations, and the corresponding brain activity mode can all be predicted from the nFC without recourse to the edge-centric formulation. Many of these derivations are based on the null hypothesis of i.i.d. Gaussian variables, incorporating the observed static spatial correlations but not the temporal ones. Under this stationarity assumption, and by invoking results from random matrix theory [16], the edge time series variability is described by the sampling distribution of the nFC (correlation) matrix, known as the Wishart distribution [17]. When tested using fMRI data from the Human Connectome Project (HCP) [18], the analytic predictions based on the null model are sufficient to replicate the main edge-centric features both qualitatively and quantitatively, as shown in Section II.

* leonardo.novelli@monash.edu

II. RESULTS

We present five main results showing that the existing findings based on edge time series [1, 2] can be derived from the (static) nFC under the null hypothesis of independent multivariate Gaussian variables. The theoretical predictions were empirically tested on 100 unrelated subjects from the HCP dataset, preprocessed with the current standard HCP pipeline, both with and without global signal regression (GSR). All the technical details are provided in the Methods section and additional evidence and visualisations are presented in the Supplementary Material, reserving the current section for a concise account of the key results.

A. The edge-centric FC matrix can be derived analytically from the node-centric FC

The eFC matrix [2] can be analytically derived from the nFC under the null hypothesis. When tested on the HCP dataset, the predicted eFC matrix achieved an average Pearson correlation of $r = 0.88$ with the empirical one ($r = 0.93$ without global signal regression (GSR); distributions shown in the Supplementary Material, Fig. S1). This is a significant improvement on the linear regression approach adopted in [2], which achieved an average Pearson correlation of $r = 0.72$ on pairs of edges not sharing any nodes, but performed poorly otherwise ($r = 0.06$). Moreover, the analytic relationship explains why the eFC is highly replicable, stable within individuals across multiple scan sessions and consistent across datasets—so long as the nFC is.

B. The edge communities can be predicted from the nFC

The eFC matrix has also been used to identify the edge communities [2]. Although these could naturally be replicated by applying the same clustering algorithm to the predicted eFC, a mathematical derivation will provide further insight. An obstacle to a full analytic approach is that the outcome of stochastic clustering algorithms cannot be entirely predicted from their input; however, it is reasonable to expect that the smaller the distance between two rows of the eFC matrix, the higher the probability that the corresponding edges would be clustered together. What does this hypothesis imply for the nodes? A proxy measure for the node similarity can be derived from the edge distances and expressed in term of BOLD signal correlations. That is, the edge communities can be predicted from the nFC alone, avoiding the memory-intensive computation of the eFC matrix and computationally-intensive clustering algorithms. (It is worth noting here that the eFC matrix scales with the fourth power of the number of regions and requires over a terabyte of memory for fine brain parcellations—for each subject.) Indeed,

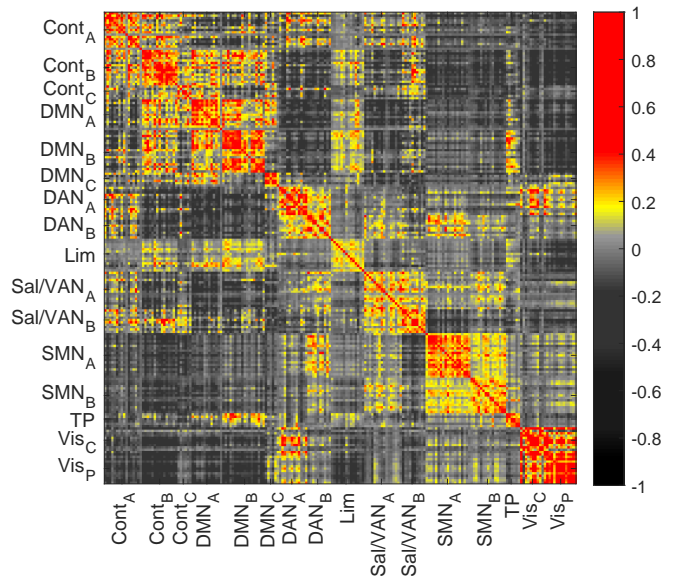


FIG. 1. Edge cluster similarity predicted from the node-centric functional connectivity (nFC), without recourse to the edge time series, the edge-centric FC matrix (eFC), nor any clustering algorithms. Compare this figure with the result published in [2, Fig.6b].

a surprisingly close match to the edge-cluster similarity matrix published in [2, Fig.6b] can be obtained by simply rearranging the rows and columns of the nFC matrix to match the ordering of the 16 networks used therein (Fig. 1). The nFC alone achieves an average Pearson correlation of $r = 0.76$ with the empirical edge-cluster similarity matrix obtained from the HCP dataset, while clustering the predicted eFC matrix achieves a correlation of $r = 0.97$ (see Supplementary Material, Fig. S2). Once again, the (static) node-centric second-order features of the BOLD signal are sufficient to replicate findings that appear at first to rely on finely tuned co-fluctuations of the edge time series.

C. The null model reproduces the high similarity of the top RSS frames to the nFC

Let us now consider the root-sum-of-squares (RSS) of the edge time series introduced in [1]. The key finding is perfectly reproduced by the null model: only a small fraction of frames exhibiting the largest RSS are required to explain a significant fraction of variance in the nFC, as well as the network’s modular structure (see Fig. 2 and Supplementary Material, Fig. S3). What is particularly remarkable is that the timing of the high-amplitude RSS events produced by the null model are arbitrary, and yet a small fraction of the edge time series corresponding to these large co-fluctuations is still sufficient to explain the observed nFC. Furthermore, the top frames of the null model also exhibit high similarity to the top frames of the real HCP data—occurring at entirely different times.

A theoretical explanation for these findings will be provided in Section II E and detailed in the Methods section. Interestingly, most of these points were also reported in [1, Fig. S4], where they were taken as evidence that the large RSS events are not fMRI artefacts. While addressing this methodological question, these observations raise a conceptual concern: if matching the timing of the RSS events is not essential and the results can be replicated by the static null model, does the edge-centric approach provide statistical information about the time-varying connectivity that cannot be explained by the static nFC? We will next address this question by examining the statistical properties of the RSS.

D. The RSS distribution is determined by the nFC eigenvalues

Having established that the large RSS events are not an exclusive feature of neural signals, let us investigate how their ubiquitous appearance can be analytically explained and why the corresponding frames account for the largest fraction of variance in the nFC. As a first step, the RSS can be computed as the squared Euclidean norm of the (z-scored) BOLD signal. In other words, although it was introduced in [1] to capture the co-fluctuations between edge time series, the RSS can also equivalently be seen, and mathematically derived, as a measure of the fluctuation of the BOLD signal amplitude over time. We can then proceed without resorting to the edge time series, which is not only convenient in practice but also shifts the conceptual focus back to the BOLD time series—which are more readily interpretable. For a large family of common (sub-Gaussian) distributions, the squared Euclidean norm of a random variable is heavy-tailed (more specifically, it is sub-exponential). Being the RSS a squared norm, large co-fluctuations are then to be expected (because of their heavy-tailed distribution), offering an explanation for the large RSS peaks observed in the BOLD time series.

In the specific case of Gaussian variables (i.e., the null hypothesis), the RSS can be expressed as a sum of Gamma-distributed variables, each related to an eigenvalue of the nFC matrix. The largest eigenvalues capture the distribution tail and including smaller eigenvalues provides an increasingly complete characterisation of the empirical RSS distribution (Fig. 3B). This distribution can be used for testing the statistical significance of the empirical RSS observed in the HCP dataset against the null hypothesis of spatially correlated noise. Fig. 3A illustrates the convergence of the empirical RSS distribution to the null distribution as more and more time frames are observed (i.e., over longer fMRI sessions). When all the 1200 time frames available in the HCP data are utilised, the null hypothesis cannot be rejected on 58% of the participants at a 5% significance level (and on 90% of the participants after the Bonferroni correction for multiple comparisons. The p-values are given by the Kolmogorov-Smirnov test).

E. The spatial mode underpinning large BOLD fluctuations is defined by the leading nFC eigenvector

Finally, high-amplitude RSS co-fluctuations were observed to be underpinned by a particular spatial mode of brain activity in which default mode and control networks are anticorrelated with sensorimotor and attentional systems [1]. This particular spatial mode was defined as the first principal component of the BOLD activity and, as such, it can be obtained as the largest eigenvector of the static nFC matrix (by a mathematical equivalence and without recourse to null models: compare Fig. 4A with [1, Fig.2E]).

The only question left to answer is whether the RSS can be predicted to peak when the BOLD activity aligns with the largest eigenvector. This can be proven to be true even without the null i.i.d. hypothesis (see Methods section) and can be intuitively understood once the RSS is seen as the fluctuation of the BOLD signal amplitude over time: high-amplitude frames have a larger variance, which is captured by a larger coefficient of the first principal component (compare Fig. 4C with [1, Fig.2C]). We can then refine our theoretical understanding of the RSS peaks: not only they occur when the Euclidean norm of the BOLD signal is large but, most likely, when the expressed spatial mode is well aligned with the leading eigenvector of the nFC (Fig. 4B). If the alignment were perfect at a given frame, the instantaneous estimate of the nFC obtained from its leading eigenvector would achieve a similarity of $r = 0.66$ (Pearson correlation coefficient) with the average nFC computed over 100 unrelated participants of the HCP dataset. However, the alignment with the leading eigenvector need not be perfect: in general, large RSS values can be expected whenever the expressed spatial mode is a mixture of the top eigenvectors (Fig. 4B). Additional principal components are expressed as more large-RSS frames are averaged, suggesting why the top 5% frames alone are sufficient for an almost perfect reconstruction of the nFC (Fig. 2). We have thus explained why the nFC estimates corresponding to frames with the largest RSS exhibit the highest similarity with the nFC. Moreover, since the nFC features multiple communities, the top frames naturally reflect this property by exhibiting high modularity (and higher values than the low frames, which are less similar to the nFC; see Supplementary Material, Fig. S3).

We intentionally postponed the analytic derivations in order to promote readability and intuition in this section. Nonetheless, all the statements made above are based on formal mathematical proofs and arguments presented in detail in the Methods section.

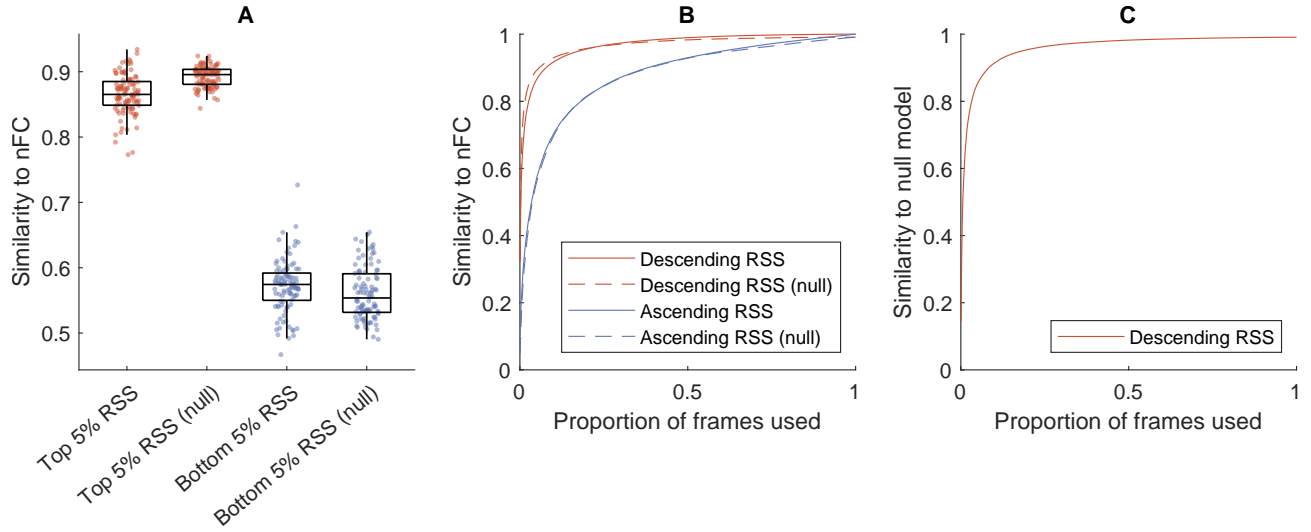


FIG. 2. **A)** The i.i.d. null model can reproduce the results published in [1, Fig.1D], despite the arbitrary timing of the simulated high-amplitude cofluctuations. Only a small fraction of frames exhibiting the largest cofluctuations root-sum-of-squares (RSS) are required to explain most of the nFC variance. The similarity is computed as the Pearson correlation coefficient between the nFC and the average FC estimated from the top and bottom 5% of the total frames. Each point corresponds to one of 100 unrelated subjects from the Human Connectome Project (HCP) dataset. **B)** The same results hold more generally when the frames are ordered according to the corresponding RSS amplitude, either in descending or ascending order. Here, the curves represent the average over 100 subjects. **C)** The findings do not depend on the timing of the high-amplitude RSS events: the top frames generated by the null model exhibit high similarity to the top frames of the real HCP data, which occur at different times.

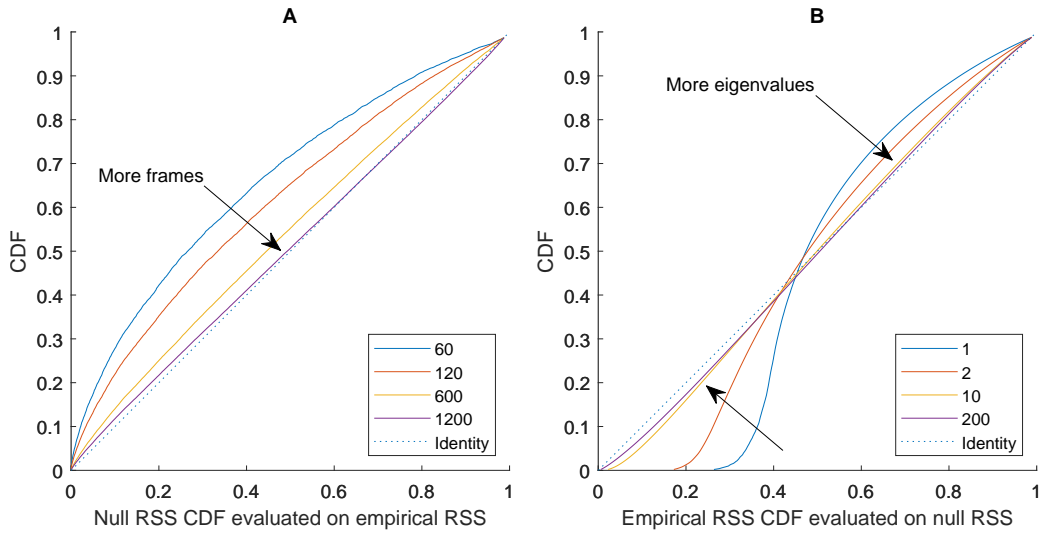


FIG. 3. **A)** The empirical RSS distribution increasingly approximates the null RSS distribution as more realisations (frames) are observed. On the horizontal axis, the cumulative distribution function (CDF) of the null RSS is evaluated for each empirical RSS observation; the CDF of the resulting distribution is plotted on the vertical axis. Identical distributions would produce points on the diagonal (dotted line). **B)** The nFC eigenvalues shape the null RSS distribution. The null RSS distribution increasingly approximates the empirical RSS distribution as more eigenvalues are considered, with the largest eigenvalues explaining most of the variance. On the horizontal axis, the cumulative distribution function (CDF) of the empirical RSS is evaluated for each null RSS observation; the CDF of the resulting distribution is then plotted on the vertical axis. Identical distributions would produce points on the diagonal (dotted line).

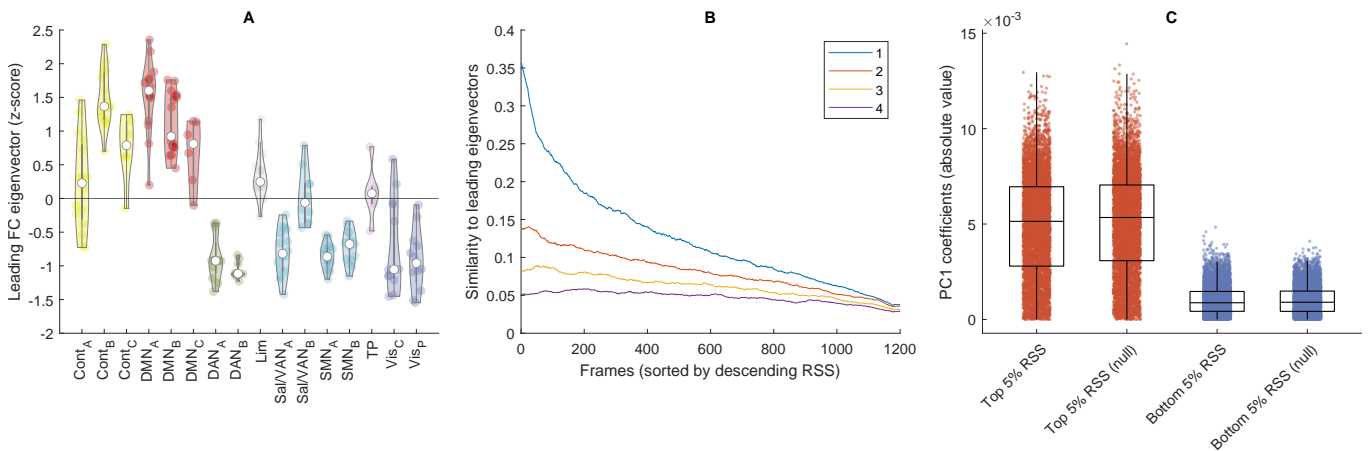


FIG. 4. **A)** The spatial mode underpinning high-amplitude cofluctuations is captured by the leading eigenvector of the nFC matrix. Compare this figure with the results published in [1, Fig.2E]. **B)** Frames corresponding to large RSS values exhibit high similarity to the leading nFC eigenvectors. The similarity is measured as the Pearson correlation between the FC estimate from a single frame and each of the estimates from the the four leading nFC eigenvectors. **C)** The i.i.d. null model reproduces the higher principal component (PC1) coefficients associated with large RSS events. Compare this figure with the results published in [1, Fig.2C].

III. DISCUSSION

We have presented ample evidence supporting the claim that the static nFC is sufficient to replicate the main resting-state findings in [1] and [2] both qualitatively and quantitatively, without relying on finely-tuned cofluctuations of the edge time series nor any other edge-centric properties. Specifically, the eFC matrix, the edge communities, the cofluctuations properties and distribution, and the corresponding brain activity mode can all be predicted from the nFC under the null hypothesis of i.i.d. Gaussian variables. The inability to reject the null hypothesis on most of the HCP 100 unrelated subjects does not support the conclusion that edge time series and eFC provide additional information beyond what is already provided by nFC. These results are not an attempt to disprove the existence of finely timed neural events—they just warn that the evidence provided by fMRI data may not be sufficient to reject simpler explanations for the edge-centric features studied in [1] and [2]. In fact, previous influential studies have raised similar warnings in the context of sliding-window approaches to time-varying FC [8, 10, 11].

However, it would be premature to conclude that the edge-centric approach has no merit, and we acknowledge the fast progress in its development and applications at the time of writing [5–7]. Particularly interesting is the influence of structural modules on the edge cofluctuations [7], which we briefly address in the Methods section. The size of the functional modules shapes the spectrum of the nFC: larger functional modules allow for larger eigenvalues, which underpin the high-amplitude cofluctuations. This offers a mathematical insight into the relationship between modular structure and large cofluctuations, and why the latter disappear if the modular

structure is disrupted. While fully addressing the latest preprints is beyond the scope of this work, it is possible that model-based approaches will reveal the role of edge-centric properties in bridging brain structure and function. Indeed, temporally-unfolded (or point-wise) dependence measures have been instrumental in studying the structure-function relationship in canonical complex systems [19, 20]; seeing the edge time series as point-wise mutual information under the Gaussian assumption could create new links to the existing literature.

It would also be unreasonable to assume that the null hypothesis of i.i.d. variables be a good description of the BOLD signal, which is slowly-varying and highly autocorrelated. Thus, the fact that such null model is able to replicate the edge-centric features in [1] and [2] could be an indication that the temporal structure of the edge time series has not been fully exploited. Indeed, besides the synchronisation of the cofluctuations across subjects watching the same movies, most of the proposed features are invariant to the exact event timing and can thus be replicated from the nFC under the i.i.d. assumption. Let us note, however, that the role of null models in time-varying FC is a matter of current debate [8, 21], and not all features that can be explained by null models are clinically irrelevant or to be dismissed. For example, using a small fraction of high-amplitude frames to approximate the nFC has been suggested as a way to compress the BOLD signal and alleviate the computational burden of analysing large fMRI datasets without compromising the prediction accuracy [22]. As a final contribution of our work, we have analytically shown that this is to be expected: the nFC captures the BOLD signal variance, which is a second order statistic and heavy-tailed (even if the BOLD signal were Gaussian). Therefore, the nFC is necessarily shaped by a few tail events corresponding to large amplitude

frames. These frames shape the leading eigenvectors of the nFC and, equivalently, the first principal components of the BOLD signal.

In conclusion, we have laid out the mathematical foundations for the edge-centric FC analysis with the goal of informing new studies, in an interplay with empirical observations and simulations. Future work could leverage this theoretical framework and direct the focus on observations that cannot be easily explained by minimal null models.

IV. METHODS

A. Definition of edge-centric FC

Functional connectivity is defined as the magnitude of the statistical dependence between pairs of brain parcels. This dependence is typically estimated from their time series (here, the BOLD signal) using the Pearson correlation coefficient. Let N be the number of parcels, T be the number of recorded frames, and $x_i = [x_i(1), \dots, x_i(T)]$ be the time series recorded from parcel i , with $1 \leq i \leq N$. The correlation between two parcels i and j can be computed as $r_{ij} = \frac{1}{T-1} \sum_t z_i(t)z_j(t)$, where z_i and z_j are their z-scored time series row vectors, i.e., $z_i = \frac{x_i - \mu_i}{\sigma_i}$ (with μ_i and σ_i indicating the time-averaged mean and standard deviation). Repeating this procedure for all pairs of parcels results in a node-by-node ($N \times N$) correlation matrix $R = [r_{ij}]$, which is an estimate of the (node-centric) functional connectivity.

The edge time series between two parcels i and j is the vector resulting from the element-wise product of z_i and z_j , which encode the magnitude of their co-fluctuations over time:

$$c_{ij}(t) := z_i(t)z_j(t). \quad (1)$$

On the other hand, the column vector of all the N^2 edge time series values at a given time t can be reshaped into a $N \times N$ matrix that is an instantaneous estimate of the dynamic functional connectivity based on a single frame.

It is also possible to go one step further and estimate the statistical dependence between each pair of edge time series, where each edge corresponds to a pair of parcels. This fourth-order statistic has been named edge functional connectivity (eFC) [2] and results in a large $N^2 \times N^2$ matrix with entries

$$eFC_{jk,lm} := \frac{\sum_t c_{jk}(t) c_{lm}(t)}{\sqrt{\sum_t c_{jk}(t)^2} \sqrt{\sum_t c_{lm}(t)^2}}. \quad (2)$$

B. Null hypothesis

Let z be the $N \times T$ (parcels \times frames) matrix of z-scored BOLD observations. Since our goal is to derive the (dynamic) edge-centric properties from the (static)

nFC matrix ($R = [r_{ij}]$), we need to define a null hypothesis that discounts any temporal dependencies but retains the observed spatial correlations in R . A simple null hypothesis on the distribution of (the columns of) z that satisfies this criterion is $Z(t) \sim \mathcal{N}(0, R)$, that is, i.i.d. multivariate Gaussian random variables (RV) with a covariance matrix R matching the observed nFC. If we denote the state of the system at time t as the column vector $z(t) = [z_1(t), \dots, z_N(t)]^\top$, the null hypothesis simply states that $z(t)$ is drawn from the same multivariate Gaussian distribution at each time t , independently of the other samples. We will denote the RV associated with the edge time series $c_{ij}(t)$ with a capital letter, i.e., $C_{ij}(t)$. In the previous section, we noted that the column vector of all the N^2 edge time series values at a given time t can be reshaped into a $N \times N$ matrix $[C_{ij}(t)]$ that provides an instantaneous estimate of the dynamic functional connectivity based on a single frame. Under the null hypothesis, this matrix is known to follow a Wishart distribution [17].

C. Derivation of edge FC

With capital letters denoting RVs, the expected sample inner product between two edge time series C_{jk} and C_{lm} (as row vectors) is

$$\begin{aligned} \mathbb{E} \left[\frac{C_{jk} C_{lm}^\top}{T} \right] &= \mathbb{E} \left[\frac{1}{T} \sum_t C_{jk}(t) C_{lm}(t) \right] \\ &= \frac{1}{T} \sum_t \mathbb{E}[Z_j(t) Z_k(t) Z_l(t) Z_m(t)] \\ &= \frac{1}{T} \sum_t (\kappa(Z_j(t) Z_k(t) Z_l(t) Z_m(t)) \\ &\quad + \mathbb{E}[Z_j(t) Z_k(t)] \mathbb{E}[Z_l(t) Z_m(t)] \\ &\quad + \mathbb{E}[Z_j(t) Z_l(t)] \mathbb{E}[Z_k(t) Z_m(t)] \\ &\quad + \mathbb{E}[Z_j(t) Z_m(t)] \mathbb{E}[Z_k(t) Z_l(t)]), \end{aligned} \quad (3)$$

where $\kappa(Z_j(t) Z_k(t) Z_l(t) Z_m(t))$ is the joint cumulant and the products involving the expectation of a single variable are equal to zero (i.e., $\mathbb{E}[Z_i(t)] = 0$) since z_i are z-scored. Under the null hypothesis, the joint cumulant is equal to zero (a property of Gaussian RVs [23]) and the terms in the sum are all equal (since the variables are i.i.d.), allowing a simplification of Eq. (3):

$$\mathbb{E} \left[\frac{C_{jk} C_{lm}^\top}{T} \right] = r_{jk} r_{lm} + r_{jl} r_{km} + r_{jm} r_{kl}. \quad (4)$$

Finally, the edge FC is obtained by normalising Eq. (4):

$$eFC_{jk,lm} = \frac{r_{jk} r_{lm} + r_{jl} r_{km} + r_{jm} r_{kl}}{\sqrt{1 + 2r_{jk}^2} \sqrt{1 + 2r_{lm}^2}}. \quad (5)$$

Note that the Gaussian assumption can be relaxed since the derivations in this section require i.i.d. RVs with the only additional constraint that $\kappa(Z_j(t) Z_k(t) Z_l(t) Z_m(t)) = 0$.

D. Derivation of edge communities

In order to formalise the intuition that two edges (jk) and $(j'k')$ with similar rows of the eFC matrix are likely to be clustered together, let us define their distance $d_{jk,j'k'}$ as the ℓ^1 norm of the difference between the corresponding rows of the (unnormalised) eFC matrix:

$$\begin{aligned}
d_{jk,j'k'} &:= \sum_{l,m=1}^N \frac{1}{T} |\mathbb{E}[C_{jk}C_{lm}^\top] - \mathbb{E}[C_{j'k'}C_{lm}^\top]| \\
&= \sum_{l,m=1}^N |r_{jk}r_{lm} + r_{jl}r_{km} + r_{jm}r_{kl} \\
&\quad - r_{j'k'}r_{lm} - r_{j'l}r_{k'm} - r_{j'm}r_{k'l}| \\
&= \sum_{l,m=1}^N |z_j z_k^\top z_l z_m^\top + z_j z_l^\top z_k z_m^\top + z_j z_m^\top z_k z_l^\top \\
&\quad - z_{j'} z_{k'}^\top z_l z_m^\top - z_{j'} z_l^\top z_{k'} z_m^\top - z_{j'} z_m^\top z_{k'} z_l^\top| \\
&= \sum_{l,m=1}^N 3|z_j(z_l^\top z_m)z_k^\top - z_{j'}(z_l^\top z_m)z_{k'}^\top|. \quad (6)
\end{aligned}$$

We now have the necessary ingredients to build a measure of similarity between the nodes, which can be used to predict the edge cluster similarity in [2]. There, the similarity between two nodes is measured as the frequency with which the corresponding edges are clustered together (having fixed the number of communities to 10). Instead of discrete assignments to 10 communities, Eq. (6) provides a continuous measure of the distance between two edges. The distance between two nodes i and j can then be defined as the sum of the distances between the edges starting from i and j :

$$\begin{aligned}
d_{i,j} &= \sum_{k=1}^N d_{ik,jk} \\
&= \sum_{k,l,m} 3|(z_i - z_j)(z_l^\top z_m)z_k^\top| \\
&\leq \|z_i - z_j\| \sum_{k,l,m} 3\|(z_l^\top z_m)z_k^\top\| \\
&= \left(\sum_t (z_i(t) - z_j(t))^2 \right)^{\frac{1}{2}} \sum_{k,l,m} 3\|(z_l^\top z_m)z_k^\top\| \\
&= ((T-1)(\text{Var}[z_i] + \text{Var}[z_j] - 2r_{ij}))^{\frac{1}{2}} \sum_{k,l,m} 3\|(z_l^\top z_m)z_k^\top\| \\
&= (1 - r_{ij})^{\frac{1}{2}} \left[(2(T-1))^{\frac{1}{2}} \sum_{k,l,m} 3\|(z_l^\top z_m)z_k^\top\| \right] \\
&\propto (1 - r_{ij})^{\frac{1}{2}}, \quad (7)
\end{aligned}$$

where we used the Cauchy-Schwarz inequality and noted that the terms in the square brackets form a constant (independent of i and j). It is then apparent that the

edge-cluster similarity [2] between nodes i and j can be approximated by the nFC. Once again, note that the Gaussian assumption can be relaxed since the derivations in this section are based on Eq. (4), which requires i.i.d. RVs with the only additional constraint that $\kappa(Z_j(t)Z_k(t)Z_l(t)Z_m(t)) = 0$.

E. Derivation of RSS from the BOLD signal

Recalling the definition of the edge time series $c_{ij}(t)$ in Eq. (1), the RSS defined in [1] can be approximated as the squared Euclidean norm of the z-scored BOLD signal, up to a constant factor:

$$\begin{aligned}
\text{RSS}(t) &:= \sqrt{\sum_{i<j} c_{ij}(t)^2} \\
&= \sqrt{\frac{1}{2} \left(\sum_{i,j=1}^N c_{ij}(t)^2 - \sum_{i=1}^N c_{ii}(t)^2 \right)} \\
&= \sqrt{\frac{1}{2} \left(\sum_{i,j=1}^N z_i(t)^2 z_j(t)^2 - \sum_{i=1}^N z_i(t)^4 \right)} \\
&= \sqrt{\frac{1}{2} \left(\|z(t)\|^4 - \sum_{i=1}^N z_i(t)^4 \right)} \\
&\approx \frac{1}{\sqrt{2}} \|z(t)\|^2. \quad (8)
\end{aligned}$$

The approximation does not rely on the i.i.d. assumption; it is valid under the Gaussian null hypothesis and, more generally, for distributions with finite kurtosis – including fMRI data. Under this assumption, $\|z(t)\|^4$ dominates $\sum_i z_i(t)^4$ in Eq. (8), as can be seen from the ratio of their (expected) values:

$$\frac{\mathbb{E}[\sum_i Z_i(t)^4]}{\mathbb{E}[\|Z(t)\|^4]} \leq \frac{\sum_i \text{Kurt}[Z_i(t)]}{N^2} \xrightarrow{N \rightarrow \infty} 0. \quad (9)$$

The approximation in Eq. (8) can be replaced by an exact equality if all the N^2 edge time series are included in the RSS definition (that is, all the (i,j) tuples, rather than only the pairs with $i < j$):

$$\text{RSS}_{\text{all}}(t) := \sqrt{\sum_{i,j} c_{ij}(t)^2} = \|z(t)\|^2. \quad (10)$$

F. Why do the top RSS frames exhibit the highest similarity to the nFC?

Having rewritten the RSS as the squared Euclidean norm (Eq. (8)), we can more easily investigate the conditions underpinning the largest RSS fluctuations. Let us

introduce the RV

$$W(t) := R^{-\frac{1}{2}}Z(t) \quad (11)$$

and let

$$R = U\Lambda U^\top \quad (12)$$

be the eigendecomposition of the covariance matrix R , with $\Lambda = \text{diag}(\lambda_1, \dots, \lambda_N)$ and U being the unitary matrix of eigenvectors (since R is symmetric). Without loss of generality, assume that the eigenvalues are sorted in descending order, such that λ_1 is the largest eigenvalue and u_1 is the corresponding leading eigenvector. The RSS can be treated as a RV and rewritten in terms of $W(t)$ and the eigenvector matrix U :

$$\begin{aligned} \text{RSS}(t) &\approx \frac{1}{\sqrt{2}}\|Z(t)\|^2 = \frac{1}{\sqrt{2}}Z(t)^\top Z(t) \\ &= \frac{1}{\sqrt{2}}W(t)^\top (R^{\frac{1}{2}})^\top (R^{\frac{1}{2}})W(t) \\ &= \frac{1}{\sqrt{2}}(W(t)^\top U)\Lambda(U^\top W(t)) \\ &= \frac{1}{\sqrt{2}}\sum_i \lambda_i [(U^\top W(t))_i]^2 \\ &= \frac{1}{\sqrt{2}}\sum_i \lambda_i \langle u_i, W(t) \rangle^2 \end{aligned} \quad (13)$$

$$= \frac{1}{\sqrt{2}}\sum_i \lambda_i \|u_i\|^2 \|W(t)\|^2 \cos^2 \Theta_i(t), \quad (14)$$

where u_i is the i -th eigenvector and $\Theta_i(t)$ is the RV representing the angle formed by the vectors u_i and $W(t)$ at time t . Also note that $\|u_i\|^2 = 1$ because U is unitary. For any realisations $w(t)$ with squared norm $\|w(t)\|^2$, an upper bound on the RSS is obtained as

$$\begin{aligned} \text{RSS}(t) &\leq \frac{1}{\sqrt{2}}\|w(t)\|^2 \max_i \lambda_i \sum_i \cos^2 \theta_i(t) \\ &= \frac{1}{\sqrt{2}}\lambda_{\max}\|w(t)\|^2, \end{aligned} \quad (15)$$

noting that

$$\sum_i \cos^2 \theta_i(t) = \sum_i \frac{\langle u_i, w(t) \rangle^2}{\|u_i\|^2 \|w(t)\|^2} = \frac{\|Uw(t)\|^2}{\|w(t)\|^2} = 1. \quad (16)$$

The upper bound is reached when $\theta_1(t) = 0$, which implies that $w(t) = c \cdot u_1$, that is, $w(t)$ is aligned with the leading eigenvector u_1 . When this happens, the BOLD signal vector $z(t')$ must also be aligned with u_1 :

$$\begin{aligned} z(t') &= R^{\frac{1}{2}}w(t') = R^{\frac{1}{2}}cu_1 \\ &= U\Lambda^{\frac{1}{2}}U^\top u_1 = c\lambda_1^{\frac{1}{2}}u_1. \end{aligned} \quad (17)$$

We can then refine our theoretical understanding of the RSS peaks: not only they occur when the Euclidean norm

of the BOLD signal is large (as per Eq. (8)) but, most likely, when the expressed spatial mode is well aligned with the leading eigenvector of the static nFC (see Fig. 4B). If the alignment were perfect at a frame t' , the instantaneous estimate of the nFC would be

$$z(t')z(t')^\top = c^2\lambda_1 u_1 u_1^\top, \quad (18)$$

i.e., an approximation of the nFC obtained from its leading eigenvector only. This approximation would achieve a similarity of $r = 0.66$ (Pearson correlation coefficient) with the average nFC computed over 100 unrelated participants of the HCP dataset (in practice, the highest similarity achieved by the top frame was $r = 0.53$). However, the alignment with u_1 need not be perfect: in general, large RSS values can be expected whenever the expressed spatial mode is a mixture of the top eigenvectors. Additional principal components are expressed as more large-RSS frames are averaged, suggesting why the top 5% frames alone are sufficient for an almost perfect reconstruction of the nFC (Fig. 2). We have thus explained why the nFC estimates corresponding to frames with the largest RSS exhibit the highest similarity with the nFC. Since the nFC features multiple communities, the top frames naturally reflect this property by exhibiting high modularity (and higher values than the low frames, which are less similar to the nFC). These results are based on Eq. (8) and hold true under the assumption of finite kurtosis (which also applies in the specific case of the null hypothesis, i.e., for Gaussian variables). The i.i.d. assumption is not required.

G. Null distribution of the RSS

The RSS can be written as a simple quadratic form $\text{RSS}(t) = \frac{1}{\sqrt{2}}\|Z(t)\|^2 = \frac{1}{\sqrt{2}}Z(t)^\top Z(t)$, which is known to follow a generalised χ^2 distribution under the null hypothesis of Gaussian variables [24]. The weights of the non-central chi-square components are proportional to the eigenvalues of the nFC matrix, i.e., $(\frac{\lambda_1}{\sqrt{2}}, \dots, \frac{\lambda_N}{\sqrt{2}})$. Another characterisation of this distribution is provided by Eq. (13): under the null hypothesis, the inner product $\langle u_i, W(t) \rangle$ follows a normal Gaussian distribution since $W(t) \sim \mathcal{N}(0, 1)$ and U is unitary. Therefore, $\langle u_i, W(t) \rangle^2$ follows a χ^2 distribution and each term $\frac{\lambda_i}{\sqrt{2}}\langle u_i, W(t) \rangle^2$ in Eq. (13) follows a $\text{Gamma}(k = \frac{1}{2}, \theta = \sqrt{2}\lambda_i)$ distribution. The RSS is thus obtained as a sum of N independent Gamma-distributed RVs, each associated with one eigenvalue of the nFC. The tail of the RSS is best approximated by the RVs associated with the largest eigenvalues (which have the largest mean and variance), while including smaller eigenvalues provides an increasingly fuller characterisation of the whole distribution (Fig. 3B). The mean and variance of the RSS can be readily obtained from the

properties of the Gamma distribution:

$$\mathbb{E}[\text{RSS}] = \frac{1}{\sqrt{2}} \sum_i \lambda_i = \frac{N}{\sqrt{2}} \quad (19)$$

$$\text{Var}[\text{RSS}] = \sum_i \lambda_i^2. \quad (20)$$

Higher moments of the RSS null distribution can be derived from its moment-generating function:

$$M_{\text{RSS}}(s) = \prod_i (1 - \sqrt{2}\lambda_i s)^{-\frac{1}{2}}. \quad (21)$$

H. On the widespread occurrence of large RSS fluctuations across datasets

The moment-generating function in Eq. (21) can be employed to show that the RSS is subexponential under the null hypothesis, which explains its heavy tail and the consequent large events [14, 15]. Specifically, the subexponential feature of the null RSS follows from the sufficient condition

$$\begin{aligned} M_{\text{RSS}-\mathbb{E}[\text{RSS}]}(s) &= \prod_i (1 - \sqrt{2}\lambda_i s)^{-\frac{1}{2}} \exp -\frac{\lambda_i s}{\sqrt{2}} \\ &\leq \prod_i \exp \lambda_i^2 s^2 = \exp s^2 \sum_i \lambda_i^2, \quad (22) \\ \forall |s| &\leq (4\lambda_{\max})^{-1}. \end{aligned}$$

However, we can expect this behaviour under the more general hypothesis that the z-scored BOLD signal is sub-Gaussian, i.e., its tail decays at least as fast as that of a Gaussian RV (including, for example, any uniformly-bounded RVs). The reason is that the square of a sub-Gaussian RV is sub-exponential, and the sum of independent subexponential RVs is also subexponential. Therefore, being the RSS closely approximated by a sum of squared RVs (as per Eq. (8)), extreme events are to be expected under the general sub-Gaussian assumption for the BOLD signal, which offers an explanation for the large RSS fluctuations observed in most fMRI datasets.

I. How do functional modules influence the edge cofluctuations?

Interestingly, Pope *et al.* [7] have recently reported a connection between the presence of structural modules and the occurrence of large events in the edge cofluctuations (RSS). Insofar as structural and functional modules are in agreement [25, 26], we can explain these findings based on the nFC spectrum. How do functional modules shape the eigenspectrum of the nFC? In the ideal case of a block-diagonal matrix (with zeroes outside the blocks), the sum of the eigenvalues corresponding to each block coincides with the block size (since the diagonal elements

are all ones and the trace is preserved under diagonalisation). As such, the largest eigenvalue is bounded by the size of the largest block, i.e., larger functional modules allow for larger eigenvalues. In turn, large eigenvalues underpin the high-amplitude cofluctuations, as shown in Section IV F. Therefore, if the size of the modules is reduced via randomisation of the structural connectivity as in [7, SI Fig. 3], the expected magnitude of the RSS cofluctuations will drop according to Eq. (15). This offers a mathematical explanation for the lower RSS event count when the modular structure is disrupted.

J. Human Connectome Project fMRI Dataset

This study used openly-available and independently-acquired resting-state fMRI (rsfMRI) data from the Human Connectome Project (HCP) S1200 release [27]. In particular, we used the “100 unrelated subjects” dataset: a subset of 100 unrelated adult participants which were pre-selected by the HCP coordinators (54% female; mean age = 29.11 ± 3.67 years; age range, 22–36 years). The HCP study was approved by the Washington University Institutional Review Board, and informed consent was obtained from all participants. All subjects were scanned on a customized Siemens 3T “Connectome Skyra” with a 32-channel head coil, housed at Washington University in St. Louis. rsfMRI data was acquired in four runs of 15 minutes over a 2-day period, with eyes open and relaxed fixation on a projected bright cross-hair on a dark background (presented in a darkened room). Resting state images were collected with the following parameters: gradient-echo EPI sequence, run duration = 14:33 min, TR = 720 ms, TE = 33.1 ms, flip angle = 52°, FOV = 208x180 mm (RO x PE), matrix = 104x90 (RO x PE), slice thickness = 2 mm, 2-mm isotropic voxel resolution, multi-band factor = 8, echo spacing = 0.58 ms, BW = 2290 Hz/Px).

K. Pre-processing and ICA-FIX denoising

Functional images in the HCP dataset were minimally pre-processed according to the pipeline described in [28]. In short, the data was corrected for gradient distortion, susceptibility distortion and motion and then aligned to a corresponding T1-weighted image with one spline interpolation step. This volume was further corrected for intensity bias, normalised to a mean of 10000, projected to the 32k_fs_LR mesh (excluding outliers), and aligned to a common space using a multi-modal surface registration.

In addition, the preprocessed rsfMRI data was cleaned of structured noise through a process that pairs independent component analysis (MELODIC) with FIX to automatically remove non-neural spatiotemporal components (trained on 25 hand-labeled HCP subjects). The FIX approach and initial results of classification accuracy are detailed in [29], and the effects of the ICA

+ FIX cleanup (and optimal methods to remove the artefactual components from the data) are evaluated in detail in [30]. The cleaning pipeline is described more comprehensively in the HCP S1200 release reference manual (<https://humanconnectome.org/study/hcp-young-adult/document/1200-subjects-data-release/>) and the preprocessing and the cleaning scripts are openly available on Github (<https://github.com/Washington-University/HCPpipelines>). The resulting ICA-FIX denoised rfMRI grayordinate surface timeseries are available as CIFTI files following the naming pattern: *REST1,2_LR,RL_Atlas_MSMAll_hp2000_clean.dtseries.nii.

The Schaefer200 parcellation was used to define 200 areas on the cerebral cortex [31]. This functional parcellation was designed to optimise both local gradient and global similarity measures of the fMRI signal and is openly available in ‘32k fs LR’ space for the HCP dataset. The nodes are mapped to the Yeo canonical functional networks [32]. The parcellated data was analysed both before and after regressing the global signal. The theoretical derivations and predictions hold and perform equally well in both cases, and we report any significant differences when they occur. Unless otherwise stated, the GSR results are shown in the figures since they are more directly comparable to those published in [1] and [2], noting in particular that GSR was performed in [1]. Despite the ICA-FIX preprocessing pipeline used here is entirely different from those employed in [1] and [2], our results are in excellent agreement with the previously published ones.

V. DATA AND CODE AVAILABILITY

The imaging data from the Human Connectome Project is publicly available and can be accessed after signing a data use agreement at <https://db.humanconnectome.org>. The analysis was performed with MATLAB (MathWorks, Inc., version 2020b) and the code is made available on Github for reproducibility (github.com/LNov/eFC).

ACKNOWLEDGMENTS

Leonardo Novelli is funded by the Australian Research Council (Ref: DP200100757). Adeel Razi is funded by the Australian Research Council (Refs: DE170100128 and DP200100757) and Australian National Health and Medical Research Council Investigator Grant (Ref: 1194910). Adeel Razi is also a CIFAR Azrieli Global Scholar in the Brain, Mind & Consciousness Program. We thank Joseph Lizier, Ben Fulcher, and James Mac Shine for their feedback on an earlier draft of this manuscript.

AUTHOR CONTRIBUTIONS

Leonardo Novelli: Conceptualization; Data curation; Formal analysis; Investigation; Software; Visualization; Writing — original draft. Adeel Razi: Conceptualization; Funding acquisition; Supervision; Writing — review & editing.

-
- [1] F. Z. Esfahlani, Y. Jo, J. Faskowitz, L. Byrge, D. P. Kennedy, O. Sporns, and R. F. Betzel, High-amplitude co-fluctuations in cortical activity drive functional connectivity, *Proceedings of the National Academy of Sciences* **117**, 28393 (2020).
- [2] J. Faskowitz, F. Z. Esfahlani, Y. Jo, O. Sporns, and R. F. Betzel, Edge-centric functional network representations of human cerebral cortex reveal overlapping system-level architecture, *Nature Neuroscience* **23**, 1644 (2020).
- [3] R. M. Hutchison, T. Womelsdorf, E. A. Allen, P. A. Bandettini, V. D. Calhoun, M. Corbetta, S. D. Penna, J. H. Duyn, G. H. Glover, J. Gonzalez-Castillo, D. A. Handwerker, S. Keilholz, V. Kiviniemi, D. A. Leopold, F. de Pasquale, O. Sporns, M. Walter, and C. Chang, Dynamic functional connectivity: Promise, issues, and interpretations, *NeuroImage* **80**, 360 (2013).
- [4] D. J. Lurie, D. Kessler, D. S. Bassett, R. F. Betzel, M. Breakspear, S. Kheilholz, A. Kucyi, R. Liégeois, M. A. Lindquist, A. R. McIntosh, R. A. Poldrack, J. M. Shine, W. H. Thompson, N. Z. Bielczyk, L. Douw, D. Kraft, R. L. Miller, M. Muthuraman, L. Pasquini, A. Razi, D. Vidaurre, H. Xie, and V. D. Calhoun, Questions and controversies in the study of time-varying functional connectivity in resting fMRI, *Network Neuroscience* **4**, 30 (2020).
- [5] R. F. Betzel, S. A. Cutts, S. Greenwell, and O. Sporns, Individualized event structure drives individual differences in whole-brain functional connectivity, *bioRxiv* 10.1101/2021.03.12.435168 (2021).
- [6] O. Sporns, J. Faskowitz, A. S. Teixeira, S. A. Cutts, and R. F. Betzel, Dynamic expression of brain functional systems disclosed by fine-scale analysis of edge time series, *Network Neuroscience* **5**, 406 (2021).
- [7] M. Pope, M. Fukushima, R. F. Betzel, and O. Sporns, Modular origins of high-amplitude co-fluctuations in fine-scale functional connectivity dynamics, *bioRxiv* 10.1101/2021.05.16.444357 (2021).
- [8] R. Liégeois, T. O. Laumann, A. Z. Snyder, J. Zhou, and B. T. Yeo, Interpreting temporal fluctuations in resting-state functional connectivity MRI, *NeuroImage* **163**, 437 (2017).
- [9] M. A. Lindquist, Y. Xu, M. B. Nebel, and B. S. Caffo, Evaluating dynamic bivariate correlations in resting-state fMRI: A comparison study and a new approach, *NeuroImage* **101**, 531 (2014).
- [10] T. O. Laumann, A. Z. Snyder, A. Mitra, E. M. Gordon, C. Gratton, B. Adeyemo, A. W. Gilmore, S. M. Nelson, J. J. Berg, D. J. Greene, J. E. McCarthy, E. Tagliazucchi, H. Laufs, B. L. Schlaggar, N. U. Dosenbach, and S. E. Petersen, On the stability of bold fMRI correlations, *Cerebral Cortex* **27**, 4719 (2017).
- [11] R. Hindriks, M. H. Adhikari, Y. Murayama, M. Ganzetti, D. Mantini, N. K. Logothetis, and G. Deco, Can sliding-window correlations reveal dynamic functional connectivity in resting-state fMRI?, *NeuroImage* **127**, 242 (2016).

- [12] J. Hlinka and M. Hadrava, On the danger of detecting network states in white noise, *Frontiers in Computational Neuroscience* **9**, 11 (2015).
- [13] A. Zalesky, A. Fornito, and E. Bullmore, On the use of correlation as a measure of network connectivity, *NeuroImage* **60**, 2096 (2012).
- [14] M. Filiassi, G. Livan, M. Marsili, M. Peressi, E. Vesselli, and E. Zarinelli, On the concentration of large deviations for fat tailed distributions, with application to financial data, *Journal of Statistical Mechanics: Theory and Experiment*, P09030 (2014).
- [15] S. Foss, D. Korshunov, and S. Zachary, Subexponential distributions, in *An Introduction to Heavy-Tailed and Subexponential Distributions* (Springer New York, New York, NY, 2013) pp. 43–74.
- [16] E. P. Wigner, Random matrices in physics, *SIAM Review* **9**, 1 (1967).
- [17] J. Wishart, The generalised product moment distribution in samples from a normal multivariate population, *Biometrika* **20A**, 32 (1928).
- [18] D. C. V. Essen, S. M. Smith, D. M. Barch, T. E. Behrens, E. Yacoub, and K. Ugurbil, The WU-Minn Human Connectome Project: An overview, *NeuroImage* **80**, 62 (2013).
- [19] J. T. Lizier, M. Prokopenko, and A. Y. Zomaya, Local information transfer as a spatiotemporal filter for complex systems, *Physical Review E* **77**, 026110 (2008).
- [20] J. T. Lizier, *The Local Information Dynamics of Distributed Computation in Complex Systems* (Springer Berlin Heidelberg, 2013).
- [21] R. Liégeois, B. T. T. Yeo, and D. V. D. Ville, Interpreting null models of resting-state functional MRI, *bioRxiv* 10.1101/2021.03.30.437514 (2021).
- [22] E. Tagliazucchi, M. Simiatchkin, H. Laufs, and D. R. Chialvo, The voxel-wise functional connectome can be efficiently derived from co-activations in a sparse spatiotemporal point-process, *Frontiers in Neuroscience* **10**, 10.3389/fnins.2016.00381 (2016).
- [23] M. Rosenblatt, Prediction and moments, in *Stationary Sequences and Random Fields* (Birkhäuser Boston, 1985) Chap. 2, p. 36.
- [24] A. Mathai and S. Provost, *Quadratic Forms in Random Variables*, *Statistics: A Series of Textbooks and Monographs* (Taylor & Francis, 1992).
- [25] C. J. Honey, R. Kotter, M. Breakspear, and O. Sporns, Network structure of cerebral cortex shapes functional connectivity on multiple time scales, *Proceedings of the National Academy of Sciences* **104**, 10240 (2007).
- [26] J. Cabral, E. Hugues, O. Sporns, and G. Deco, Role of local network oscillations in resting-state functional connectivity, *NeuroImage* **57**, 130 (2011).
- [27] D. C. V. Essen, S. M. Smith, D. M. Barch, T. E. Behrens, E. Yacoub, and K. Ugurbil, The wu-minn human connectome project: An overview, *NeuroImage* **80**, 62 (2013).
- [28] M. F. Glasser, S. N. Sotiropoulos, J. A. Wilson, T. S. Coalson, B. Fischl, J. L. Andersson, J. Xu, S. Jbabdi, M. Webster, J. R. Polimeni, D. C. V. Essen, and M. Jenkinson, The minimal preprocessing pipelines for the human connectome project, *NeuroImage* **80**, 105 (2013).
- [29] G. Salimi-Khorshidi, G. Douaud, C. F. Beckmann, M. F. Glasser, L. Griffanti, and S. M. Smith, Automatic denoising of functional MRI data: Combining independent component analysis and hierarchical fusion of classifiers, *NeuroImage* **90**, 449 (2014).
- [30] L. Griffanti, G. Salimi-Khorshidi, C. F. Beckmann, E. J. Auerbach, G. Douaud, C. E. Sexton, E. Zsoldos, K. P. Ebmeier, N. Filippini, C. E. Mackay, S. Moeller, J. Xu, E. Yacoub, G. Baselli, K. Ugurbil, K. L. Miller, and S. M. Smith, ICA-based artefact removal and accelerated fMRI acquisition for improved resting state network imaging, *NeuroImage* **95**, 232 (2014).
- [31] A. Schaefer, R. Kong, E. M. Gordon, T. O. Laumann, X.-N. Zuo, A. J. Holmes, S. B. Eickhoff, and B. T. T. Yeo, Local-global parcellation of the human cerebral cortex from intrinsic functional connectivity MRI, *Cerebral Cortex* **28**, 3095 (2018).
- [32] B. T. T. Yeo, F. M. Krienen, J. Sepulcre, M. R. Sabuncu, D. Lashkari, M. Hollinshead, J. L. Roffman, J. W. Smoller, L. Zöllei, J. R. Polimeni, B. Fisch, H. Liu, and R. L. Buckner, The organization of the human cerebral cortex estimated by intrinsic functional connectivity, *Journal of Neurophysiology* **106**, 1125 (2011).
- [33] M. Rubinov and O. Sporns, Weight-conserving characterization of complex functional brain networks, *NeuroImage* **56**, 2068 (2011).

SUPPLEMENTARY MATERIAL

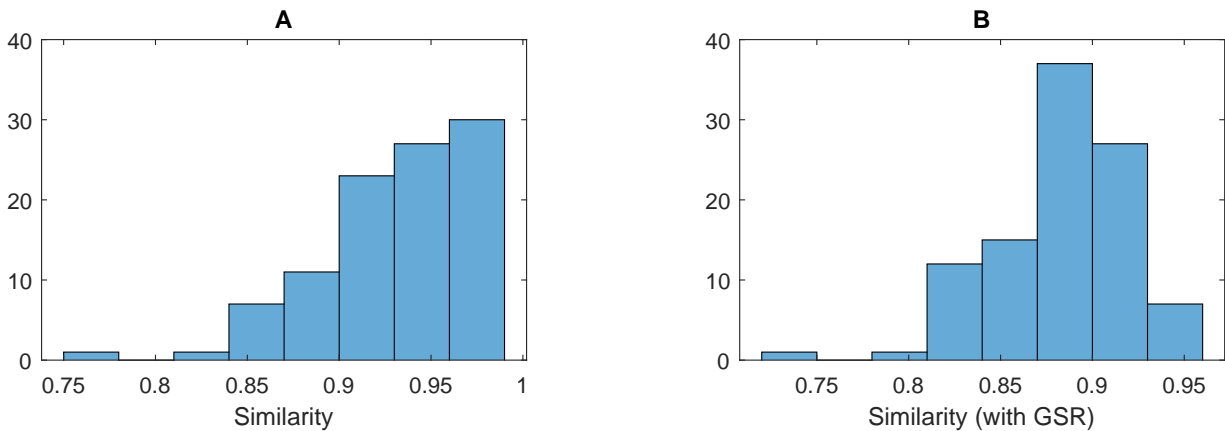


FIG. S1. **A)** Average similarity (Pearson correlation coefficient) between the empirical and predicted eFC matrices. The distribution is computed across 100 unrelated HCP participants, with an average correlation of $r = 0.93$. **B)** After global signal regression (GSR), the average correlation is $r = 0.88$.

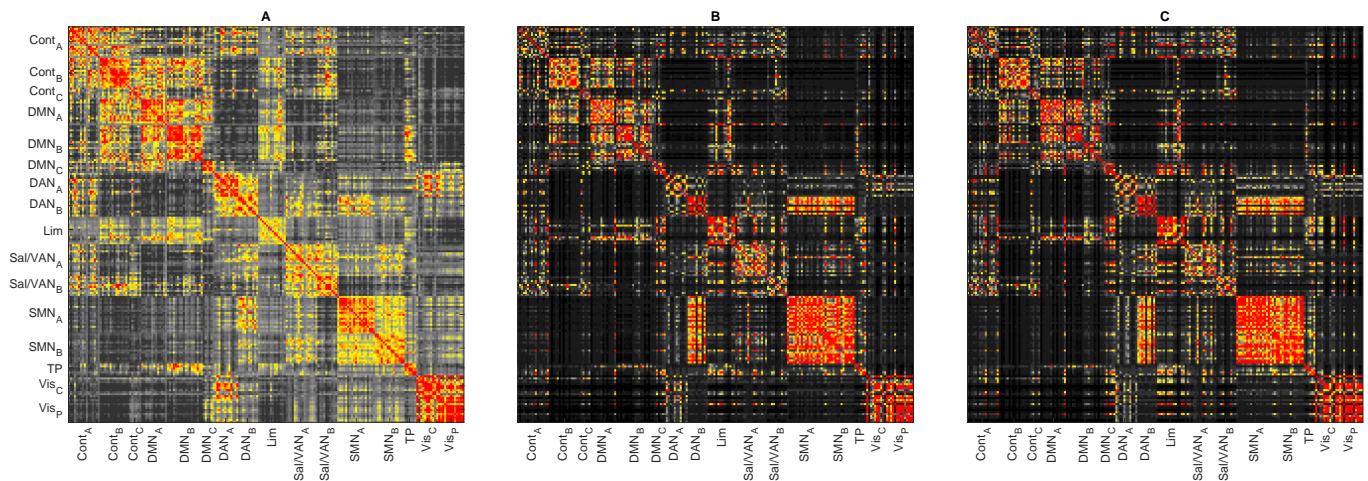


FIG. S2. **A)** The average nFC across 100 unrelated HCP participants. **B)** The empirical edge-cluster similarity as defined in [2]. Briefly, the eFC matrix is clustered using the k-means algorithm; the edge labels are then reshaped into an $N \times N$ matrix where each (i, j) entry represents the community label of the edge linking i to j ; finally, the similarity of edge communities involving nodes i and j is computed by comparing the corresponding columns and stored in the edge-cluster similarity matrix shown here. The Pearson correlation coefficient with the average nFC matrix is $r = 0.76$. **C)** The edge-cluster similarity computed on the analytically-predicted eFC matrix. The Pearson correlation coefficient with the empirical edge-cluster similarity matrix is $r = 0.97$.

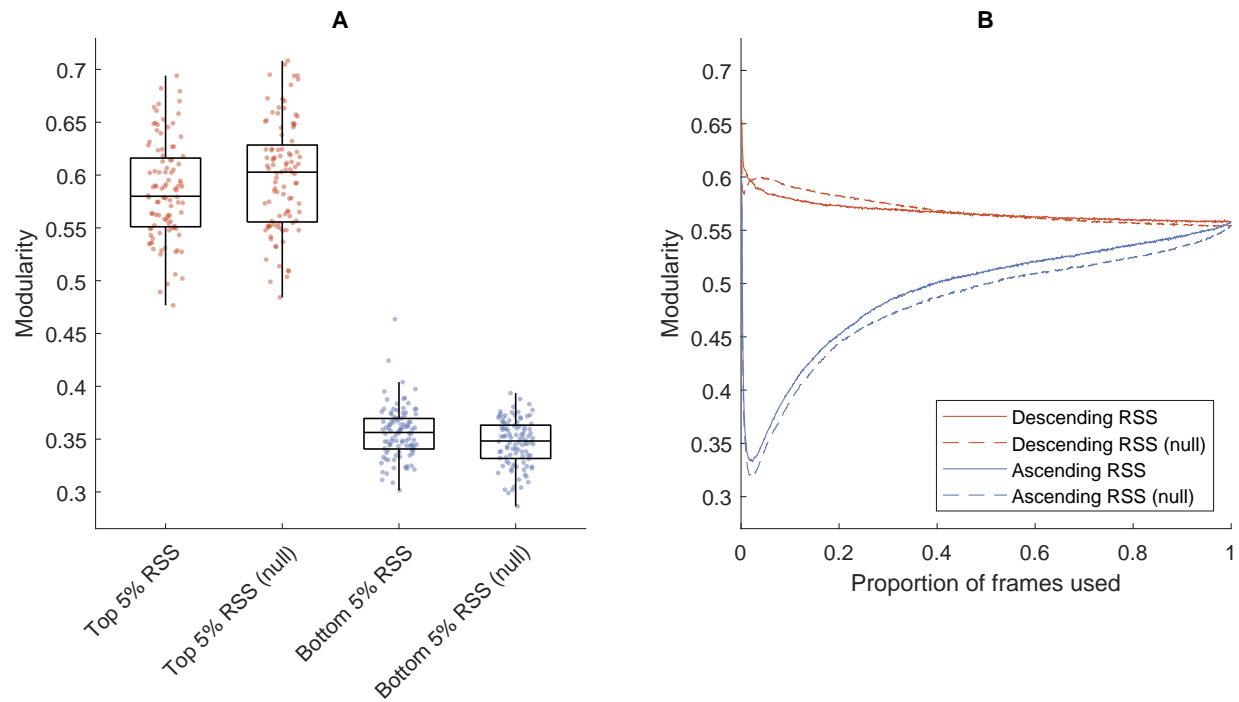


FIG. S3. Network modularity can be interpreted as a measure of the segregation between the network systems. We employed the q^* variant of modularity, which has been shown to be well suited for use with correlation matrices [33]. **A**) We first checked that our results matched the finding published in [1, Fig. 1E]: the networks estimated using the top 5% of frames exhibited much higher modularity than those estimated using the bottom 5% of frames. Then, we repeated the same analysis on synthetic time series to show that the null model can accurately replicate this result. Each point corresponds to one of 100 unrelated subjects from the Human Connectome Project (HCP) dataset. **B**) The same results hold more generally when the frames are ordered according to the corresponding RSS amplitude, either in descending or ascending order. Here, the curves represent the average over 100 subjects.